Synthesis and Characterization of Single-Domain Monocrystalline Magnetite Particles by Oxidative Aging of Fe(OH)2

ARTICLE *in* THE JOURNAL OF PHYSICAL CHEMISTRY C · MARCH 2008

Impact Factor: 4.77 · DOI: 10.1021/jp711990f

5 AUTHORS, INCLUDING:

Fernando Vereda
University of Granada
23 PUBLICATIONS **363** CITATIONS
SEE PROFILE

Juan de Vicente
University of Granada
84 PUBLICATIONS **1,660** CITATIONS
SEE PROFILE

Maria del Puerto Morales
Instituto de Ciencia de Materiales de Madrid
254 PUBLICATIONS **7,963** CITATIONS
SEE PROFILE

Roque Hidalgo-Alvarez
University of Granada
265 PUBLICATIONS **4,224** CITATIONS
SEE PROFILE

Synthesis and Characterization of Single-Domain Monocrystalline Magnetite Particles by Oxidative Aging of $Fe(OH)_2$

Fernando Vereda,*,† Juan de Vicente,† María del Puerto Morales,‡ Fernando Rull,§ and Roque Hidalgo-Álvarez†

Grupo de Física de Fluidos y Biocoloides, Departamento de Física Aplicada, Facultad de Ciencias, Universidad de Granada, Granada E-18071, Spain, Instituto de Ciencia de Materiales de Madrid, CSIC, C/ Sor Juana Inés de la Cruz 3, 28049 Cantoblanco, Madrid, Spain, and Departamento de Física de la Materia Condensada, Cristalografía y Mineralogía, Facultad de Ciencias, Universidad de Valladolid, Real de Burgos s/n, 47011, Valladolid, Spain

Received: December 21, 2007; In Final Form: January 30, 2008

We report the fabrication of highly crystalline magnetite particles with a uniform morphology and a relatively uniform average size of 54 nm. Particles were fabricated by oxidation of $Fe(OH)_2$ by nitrate in basic aqueous media. Characterization of the particles by means of transmission electron microscopy, Raman spectroscopy, X-ray and electron diffraction, and magnetometry showed that they were octahedral magnetic monodomains of highly stoichiometric magnetite (unit formula was estimated to be $Fe_{2.985}O_4$), with room-temperature ferrimagnetic behavior and a saturation magnetization of 81.6 emu/g.

1. Introduction

The fabrication of magnetite micro and nanoparticles has attracted a lot of attention, mainly because of their relevance in the development of numerous applications. These include recording media, multiple technical applications of magnetic fluids, such as seals, dampers or loudspeakers, and many biomedical applications,[1] such as biomolecule separation, drug targeting, contrast agents for NMR, or magnetic hyperthermia.

For particles of a given composition and at a given temperature, size is probably the most important parameter among those that rule their behavior, as well as the behavior of fluids prepared with them. Particle size will determine if the particle is a single magnetic domain, if it is composed of multiple domains, or if it is superparamagnetic. This, in turn, will affect the magnetization curve of the particles and, for instance, the magnitude of the losses when they are exposed to an alternating magnetic field. When particles are dispersed in a liquid, size will determine their facility to diffuse (the typical diffusion time scales as $t_{diff} \propto a^3$, where a is the particle radius) and to sediment ($t_{sed} \propto a^{-1}$). The dipolar interaction between particles also has a strong volume dependence ($E_{dipolar} \propto a^3$) so that particle size will determine the extent of the response of the magnetic fluid to an external magnetic field.

The size of the constituting magnetic particles is the main difference between the two basic types of magnetic suspensions: ferrofluids (FFs) and magnetorheological fluids (MRFs). Ferrofluids are usually prepared by dispersing sterically stabilized nanometric (∼10 nm) magnetic particles in a polar fluid.[2] Because of the small size of the particles, sedimentation is not a problem, but for the same reason, the magnetorheological response is relatively weak. Magnetorheological fluids are usually dispersions of much larger magnetic particles (∼1 μm). In this case, the magnetic response is strong and leads to dramatic changes in the mechanical properties of the fluids, but due to the large size and density of the particles, sedimentation is an issue. Particles of 50−100 nm diameter would make possible the preparation of fluids relatively resistant to sedimentation and with a significant response to moderate magnetic fields. Such fluids would not be considered classical FFs nor MRFs.

Furthermore, it has been reported that particle sizes in the range of 20−100 nm are highly desirable for magnetic hyperthermia, and Daou et al.[3] pointed out the limited success to date in the fabrication of monodisperse particles in that range. Those authors succeeded in the synthesis of particles of 39 nm with a good monodispersity by means of a coprecipitation method followed by a hydrothermal treatment. Ma et al.[4] studied a number of suspensions, each one of them prepared with magnetite particles of a particular characteristic size. Sizes ranged from 7.5 to 416 nm. The authors found that the particles that most efficiently converted the energy of a 32.5 kA/m, 80 kHz AC magnetic field into heat were those of 48 nm.

As a possible method for the fabrication of magnetite particles in the 50 to 100 nm range, we decided to revisit the oxidative aging of $Fe(OH)_2$. According to Domingo et al.,[5] it was Baudisch who in 1922 established the standard procedure for the fabrication of magnetite by oxidation of Fe^{2+} in the presence of nitrate. The method proved to be especially suitable for the fabrication of spinel iron oxides,[5] such as magnetite[6] and a variety of ferrites.[7−9] Proper control over the pH and nature and concentration of the oxidant also allows for the fabrication of particles of iron hydroxides.[10]

In 1980, Sugimoto and Matijević[6] published a comprehensive study on the fabrication of magnetite particles of a wide range of sizes (0.03 to 1.1 μm) by means of oxidation of $Fe(OH)_2$ by KNO_3. The size and morphology of the particles were strongly dependent on the initial pH of the reactant mixture. A small excess of Fe^{2+} resulted in the formation of relatively large (0.4−1.1 μm) spherical particles, whereas an excess of OH^- led to

* To whom correspondence should be addressed. Tel.: +34 958246175. Fax: +34 958243214. E-mail: fvereda@ugr.es.
† Universidad de Granada.
‡ Instituto de Ciencia de Materiales de Madrid.
§ Universidad de Valladolid.

10.1021/jp711990f CCC: $40.75
Published on Web 03/21/2008

the growth of smaller (0.03−0.1 μm) cubic particles. The reason for the different morphology was the mechanism of growth. A small excess of Fe^{2+} fixed the pH of the mixture close to the isoelectric point of magnetite and allowed the growth by aggregation of minuscule primary particles. An excess of OH^- shifted the pH to larger values and led to the charging of the surface of the growing particles. In this case, particles grew by molecular addition.

Sugimoto and Matijević obtained particles with sizes in the range of interest (50−100 nm) when the fabrication was carried out in an excess of OH-, but their article focused mainly in the spherical particles that grew in excess Fe^{2+}. Synthesis of magnetite by oxidation of $Fe(OH)_2$ with nitrate in basic aqueous media has been carried out by other groups. Domingo et al.[11] studied in detail the morphological properties of magnetite particles also fabricated by oxidation of $Fe(OH)_2$ by nitrate. They also focused on particles fabricated in excess Fe^{2+}, but they mentioned the observation of octahedral particles when the synthesis was carried out in a relatively small excess of OH^-, and surprisingly, even in one sample that was fabricated in an excess of Fe^{2+} of 0.01 M. At a larger excess of OH^-, isometric microcrystals were observed. The work focused almost completely in the morphology of the particles with no mention to the structural or magnetic properties. They do point out, however, that their particles were all "polycrystalline". In contrast with Sugimoto's work, they did not observe spherical particles when the reactant mixture had a small excess of Fe^{2+}. Reasons for this might be that they used $FeCl_2$ instead of $FeSO_4$ as the source of Fe^{2+} and worked at higher concentrations of $Fe(OH)_2$. Spiers et al.[12] fabricated particles with cubic and octahedral morphology and sizes that ranged between 40 and 320 nm. The authors then converted these particles into microspheres by means of ultrasonic atomization. Ma et al.[4] fabricated 4 different batches of magnetite particles with sizes of 46, 81, 282, and 416 nm. Not much detail was given about the synthesis process, but from micrographs that show the morphology of the particles, one can infer that those of 46, 81, and 282 nm of average size were synthesized in basic media. Zhang et al.[13] synthesized particles with an average size of 50 nm. Their particles look quite homogeneous in size and morphology, although a histogram was not presented, and the description of the fabrication process was not complete. Furthermore, refinement of the lattice parameter resulted in a lattice constant $a = 8.322$ Å, which would correspond to a nonstoichiometric form of magnetite[14] and is actually closer to the lattice parameter of maghemite. Devouard et al.[15] synthesized magnetite particles to compare them with those of bacteriological origin. Specific details of the preparation process are not given, although again, one can infer from the size and morphology of the particles that they were made in basic media.

Even though the basics of the synthesis method are known, we report specific conditions that resulted in the formation of octahedral monodomain monocrystalline magnetite particles, together with a relatively thorough characterization of them. These particles showed relatively good monodispersity and a stoichiometry close to the theoretical one of magnetite. Magnetic properties of the particles have been studied for the powder as prepared and after being randomly dispersed in a silica matrix obtained by neutralization of sodium silicate solutions with hydrochloric acid. Their magnetic behaviors were studied as a function of temperature in order to clarify the different contributions to the anisotropy as the origin of the coercivity.

2. Experimental Section

2.1. Synthesis of Magnetite Particles. Ultrapure distilled water (Milli-Q Academic, Millipore) was employed for the preparation of all solutions and for the washing of the magnetic precipitate after the synthesis process. We followed the method described by Sugimoto and Matijević[6] in 1980. This method relies on the oxidation of a $Fe(OH)_2$ gel in the presence of KNO_3 at 90 °C. Specifically, 1.948 g of KOH (90%, Panreac, chemically pure) were dissolved in water to a total volume of 12.5 mL. This solution, together with 25 mL of KNO_3 (Scharlau, Spain, ultrapure) 2 M, was added to 200 mL of water. The resultant solution was purged with N_2 for 1 h. Another solution was then prepared by adding water that had also been purged with N_2 for 1 h to 1.737 g of $FeSO_4 \cdot 7H_2O$ (Sigma Aldrich, reagent grade). The full volume of the $FeSO_4 \cdot 7H_2O$ solution was mixed with the KOH and KNO_3 solution. The mixture, which turned green at that point, was purged with N_2 for 60 more seconds. The stopper and the glass tube that were being used to introduce the N_2 flow were then removed, and the flask was tightly closed with a screw cap and placed in a water bath that had been preheated to 90 °C. The flask was left in the bath for 4 h. After that time, the flask was taken out of the bath and cooled down with ice water. The black precipitate was then washed several times with water until the conductivity of the supernatant was lower than 2 μS/cm. We used a permanent magnet to speed sedimentation of the black precipitate and facilitate the washing process. The precipitate was then washed one more time with absolute ethanol (Scharlau, reagent grade) and stored in ethanol.

Note that in this particular process, the final reactant mixture had a concentration of $FeSO_4 \cdot 7H_2O$ of 0.025 M, a concentration of KNO_3 of 0.200 M and a concentration of KOH of 0.125 M. Taking into account that the formation of $Fe(OH)_2$ can be described by the following chemical equation

$$2KOH_{(aq)} + FeSO_{4(aq)} \rightarrow Fe(OH)_{2(s)} + 2K^+_{(aq)} + SO_4^{2-}{}_{(aq)}$$

the reactants concentrations given above led to a concentration of $Fe(OH)_2$ of 0.025 M and to an excess of OH^- of 0.075 M.

2.2. Powder Samples. Powders were obtained by drying aliquots of the suspensions of magnetite in ethanol at 40 °C in air. Some of the magnetite powder was also converted to maghemite by heating it at 300 °C in air for 12 h. The powder, which was originally black, turned a dark brown reddish color. The maghemite powder was used to test our unit-cell refinement method.

2.3. Electron Microscopy and Histogram Generation. For transmission electron microscopy (TEM) observation, droplets of the suspensions of magnetite in ethanol were dried on top of graphite coated copper grids. Droplets were dried in air, and samples were observed in a STEM Philips CM20 operating at 200 kV. Selected area electron diffraction (SAED) was used to study the crystallinity of individual particles.

TEM micrographs show 2-D projections of the particles. Because most of the particles were octahedra, these projections vary in shape depending on the particular orientation of the particle. For consistency, we decided to measure the longest dimension of those particles that were individually distinguishable in the TEM micrographs. This should provide an estimate of the average distance between opposite vertices of the octahedral particles.

2.4. X-ray Powder Diffraction, Unit Cell Refinement and Grain Size Estimation. X-ray powder diffraction spectra were obtained in a Bruker D8 Advance diffractometer at room

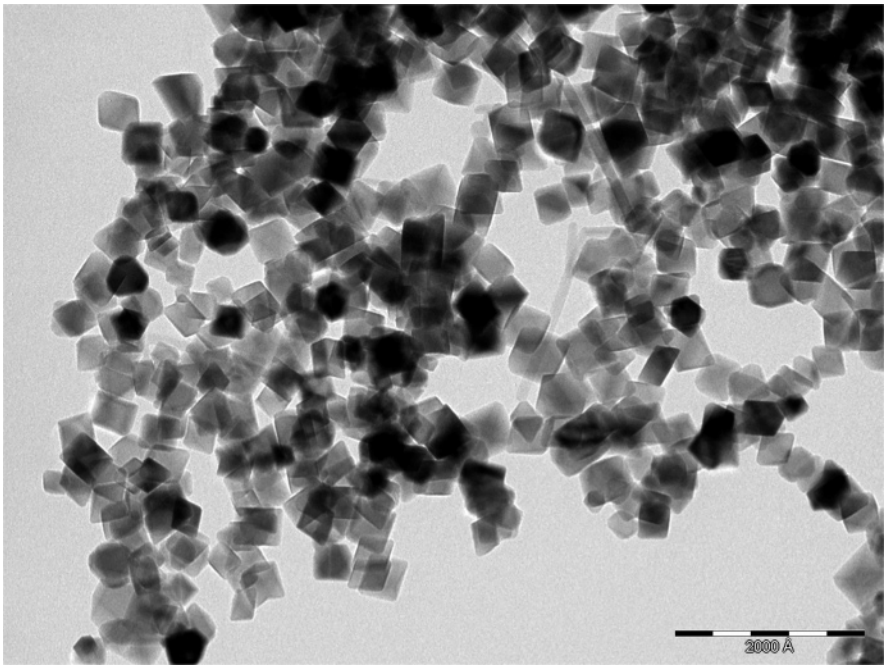

Figure 1. Transmission electron micrograph of magnetite particles fabricated by oxidation of $Fe(OH)_2$ in the presence of KNO_3 0.2 M and an excess of OH^- of 0.075 M. Concentration of $Fe(OH)_2$ was 0.025 M.

temperature. Diffraction patterns were recorded at room temperature. We scanned at a rate of 0.15 °/minute and recorded a point every 0.02°. The two lines of the Cu Kα radiation were utilized.

The freely available software Celref[16] was used for the unit cell refinement of the samples. Refinement was performed in the Fd3m space group with a fixed X-ray wavelength of 1.5418 Å, which is the average of the two lines of the Cu Kα radiation. For each sample, we tried at least 6 refinement runs, each one of them with a different starting unit cell parameter. In some runs, the positions of the peaks in the powder spectrum were found manually, whereas in others, we let the peak finder tool of the software find the peaks. The standard deviation obtained from the 6 refinement runs was taken as the error of the unit cell parameter.

Assuming that the broadening of the powder diffraction peaks was due only to the crystallite size and the instrumental broadening of the diffractometer, we used the Scherrer equation[17] to estimate the size of the crystallites:

$$L = 0.9\,\lambda\,/(B\cos\theta) \qquad (1)$$

where L is the apparent size of the crystallites, λ is the wavelength of the X-ray radiation, B is the full width at half-maximum (fwhm) of a given powder diffraction peak (in radians), and θ is the angle at which that peak is centered. The fwhm of three peaks of each spectrum was calculated after stripping the Kα-2 radiation of the spectra and removing the background with the X-Powder software.[18] Therefore, peak widths due only to the Kα-1 wavelength ($\lambda = 1.5406$ Å) were used in eq 1. The fwhm was corrected for instrumental broadening with the equation $B = (B^2_1 - B^2_{SiC})^{1/2}$, where B_1 is the fwhm of a given magnetite diffraction peak, and B_{SiC} is that of a diffraction peak taken for a SiC sample with a known average crystallite size larger than 10 μm.

2.5. Raman Spectroscopy. A micro-Raman study was performed on the powdered samples of magnetite and maghemite. The spectrometer used was a HoloSpec from Kaiser Optical Systems using a He−Ne laser at 632.8 nm as excitation source. Spectra were obtained under very low laser power (<1mW) on the sample in order to avoid thermal damage, using a LW 50× objective. Under these conditions, spectra show, in general, low signal-to-noise ratio. The spectral resolution used was 6 cm^{-1} over the spectral range 200−2700 cm^{-1}.

2.6. Magnetometry. Magnetization of the samples as a function of the applied magnetic field was measured in a vibrating sample magnetometer MLVSM9 MagLab 9 T, Oxford Instrument. The powder was pressed into a plastic tube in such a way that the axial ratio of the resulting sample was >5. As a consequence, the need to correct for sample shape demagnetizing effects was removed. Magnetization as a function of the field was measured after applying a maximum field of 800 kA/m at temperatures that ranged from room temperature down to 5 K. Saturation magnetization (M_s), was obtained by extrapolation to zero the magnetization values in the high field range versus the inverse of the applied field (1/H).

Magnetic particles were randomly dispersed and immobilized in a silica network following a procedure already published.[19] Sodium silicate (Panreac) and HCl (37%, Panreac) were simultaneously added to an aqueous solution containing 10 mg of iron oxide particles that had been previously dispersed in an ultrasonic bath. This solution was vigorously mechanically stirred to avoid local changes in pH during the formation of the precursor sol. The pH was controlled until a pH of 5 was reached. Then, the precursor sol was maintained in the ultrasonic bath until gelation occurred. The gel was washed with distilled water and dried at room temperature. The gel provided the network that kept the particles apart. The optimum pH to obtain a homogeneous coating and dispersion was chosen around 5, in accordance with the isoelectric points of silica (pH = 3) and iron oxide (pH = 7).[20] The resulting volume fraction (ratio between the volume of the iron oxide and the total volume) was approximately 0.001.

3. Results and Discussion

3.1. Particle Morphology and Size. Transmission electron micrographs (see Figure 1) showed that our sample was mostly

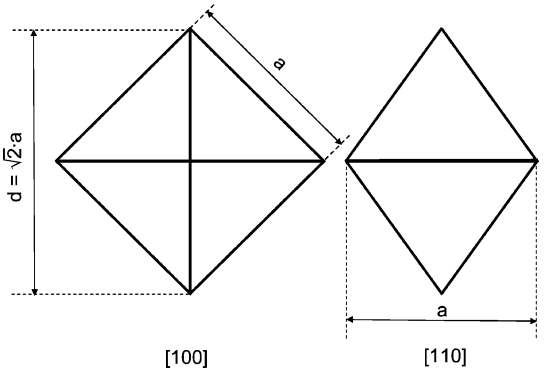

Figure 2. Views of a regular octahedron along two different directions. The projection is a square when the tetrahedron is viewed along the [100] direction, and a rhomb when it is viewed along one of the [110] axes. To obtain information about particle size, the distance between opposite vertices (*d*) was measured in the TEM micrographs.

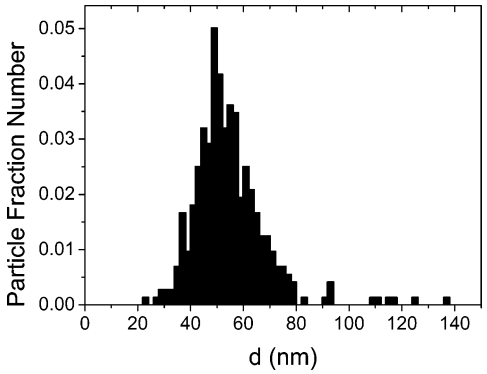

Figure 3. Size distribution of magnetite particles. We measured the distance between opposite vertices (*d* in Figure 2) of 359 octahedral particles.

constituted by octahedral particles. This is the main theoretical morphology of magnetite crystals,[11] and therefore, the particle morphology suggested that each particle was a single crystal. Because of their shape and the nature of TEM imaging, particles could appear as rhombs, squares, or even hexagons if they are viewed along the [110] the [100] or the[111] directions, respectively (Figure 2). As was explained above, we measured the longest dimension of each particle as it appeared in the TEM micrographs. This measurement yielded an estimate of the distance between opposite vertices of the octahedra, i.e., of the distance *d* in Figure 2. The result of measuring 359 particles is shown in the histogram in Figure 3. The average value of *d* was found to be 54 ± 14 nm.

3.2. Structural Characterization. Figure 4 shows the X-ray powder diffraction spectra obtained for the magnetite and the maghemite samples. All of the diffraction peaks of the magnetite spectrum could be indexed according to the inverse spinel structure of magnetite. No peaks that could be assigned to hematite or iron hydroxides were observed. The maghemite sample showed three additional low-intensity reflections at $2\theta = 15.1°$, 24.0°, and 26.2°, which can be assigned to the structure of maghemite.[21] The presence of these peaks suggests ordering of the cation vacancies and a lowering of the symmetry from cubic to tetragonal.[22,23]

Even though the additional peaks that could be assigned to maghemite were not observed in the magnetite sample, the presence of maghemite cannot be ruled out. The reason for this is that maghemite can also present a cubic structure with the same space group as magnetite (Fd3m) if the cation vacancies are randomly distributed.[22,24] Furthermore, the additional peaks

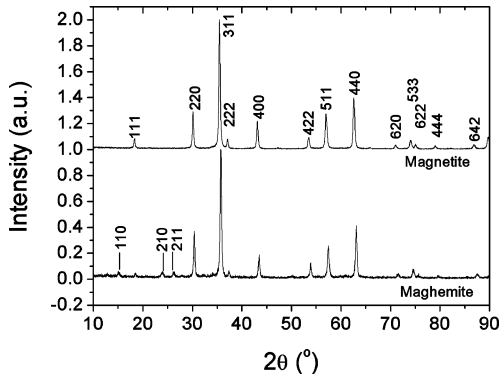

Figure 4. X-ray powder diffraction spectra of the magnetite and maghemite samples. Peaks that were indexed in the maghemite spectrum did not appear in that of magnetite.

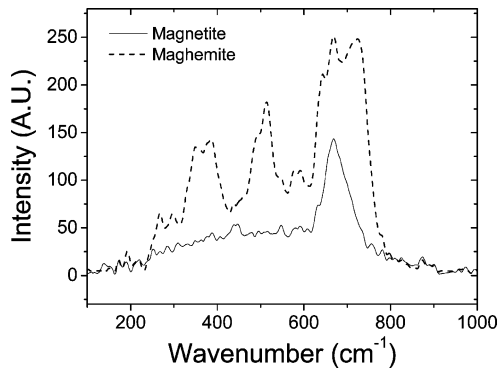

Figure 5. Raman spectra of the magnetite and the maghemite samples.

present in the maghemite sample due to the ordering of the vacancies are inherently weak.

Raman spectroscopy is commonly used to distinguish between magnetite and maghemite.[3,25] Magnetite presents a strong line at approximately 670 cm^{-1} due to the A_{1g} transition and a weaker one at 540 cm^{-1} that has been assigned to the T_{2g} transition.[26] Maghemite presents three strong bands at 350, 500, and 700 cm^{-1} that have been assigned to the T_1, E, and A_1 transitions, respectively.[27] Figure 5 shows the Raman spectrum of the magnetite and the maghemite samples. The spectrum of our magnetite sample presents only one band centered at 668 cm^{-1}, and no signs of the maghemite bands.

Another way to discriminate between magnetite and maghemite is to calculate the unit cell parameter (*a*) from the powder diffraction spectra. Refinement of the unit cell parameter for both samples gave a result of $a = 8.393 \pm 0.002$ Å for the magnetite sample and of $a = 8.345 \pm 0.002$ Å for the maghemite sample. These values compare well with tabulated data for magnetite (8.396 Å) and maghemite (8.346 Å).[6,3,23] Furthermore, the unit cell parameter provides information about the stoichiometry of the magnetite sample. Magnetite (Fe_3O_4) can oxidize to maghemite (γ-Fe_2O_3) in a process that involves oxidation of the Fe^{2+} cations and the creation of lattice vacancies. Since the structure of γ-Fe_2O_3 is closely related to the spinel structure of magnetite, the unit formula of maghemite is sometimes expressed as $Fe_{2.67}O_4$. This expression shows explicitly that all of the iron is in the form of Fe^{3+} and that, compared to magnetite, there is a deficit of 0.33 irons per unit formula. In general, non-stoichiometric magnetite, or magnetite that has been partially oxidized and presents some vacancies, can be expressed as $Fe_{3-\delta}O_4$. Stoichiometric magnetite corresponds to $\delta = 0$, whereas stoichiometric maghemite corresponds to $\delta = 1/3$. It has been observed that for intermediate products, the unit cell parameter *a* decreases linearly[14] with increasing δ.

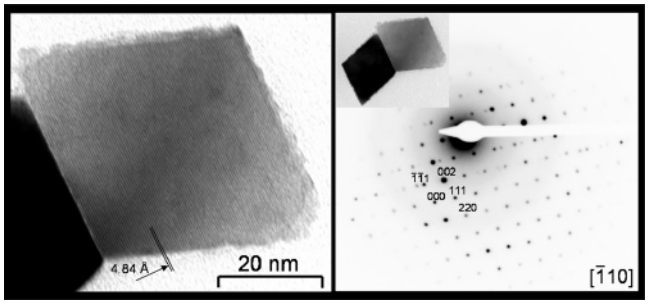

Figure 6. Left: High-resolution TEM micrograph of an octahedron in a twinned magnetite crystal. The twinned crystal is formed by two octahedra that share a (111) plane. Right: resulting SAED pattern of the dark tetrahedron shown in the insert (right).

TABLE 1: Summary of Crystallite Sizes for the Magnetite Sample[a]

2θ (°) (reflection)	crystallite apparent size, L (nm)
35.46 (311)	30.7
57.01 (511)	26.3
62.60 (440)	29.9

[a] Sizes were calculated by applying the Scherrer equation (eq 1) to three diffraction peaks (2θ = 35.46°, 57.01° and 62.60°) of the magnetite sample. Instrumental broadening was corrected using a SiC sample with a known average crystallite size greater than 10 μm. For the correction, we used the peaks at 2θ = 36.60°, 57.20°, and 60.0° of the SiC diffraction spectrum.

Yang et al.[14] observed a decrease of 0.20 Å of the lattice parameter per vacancy. From that information, we estimated that $\delta = 0.015$ for our magnetite sample, so that the unit formula would be $Fe_{2.985\pm0.010}O_4$. This is evidence that the synthesis method led to the formation of magnetite particles of good stoichiometry.

The crystallinity of the magnetite particles was also studied. Figure 6 shows a high-resolution TEM micrograph of an octahedral particle (left) and a SAED pattern (right) of the particle that appears darker in the insert. The micrograph shows that interference fringes regularly occupy the full area of the particle, which indicates that the particle is a single crystal. Distance between consecutive fringes was estimated to be 4.84 Å, which is in good agreement with the (111) interplanar distance of the magnetite structure (4.847 Å). The diffraction pattern is characteristic of a single crystal. A few less intense spots due to diffraction by the lighter octahedron of the insert are also visible. The pattern was indexed on the basis of the Fd3m space group. Calculation of the zone axis based on the indexation confirms that the particle was observed along one of the [110] axes.

The X-ray powder spectra also provided information on the crystallinity of the sample. Table 1 shows the crystallite sizes calculated from three different peaks of the powder diffraction spectrum of the magnetite sample. It should be recalled that the apparent crystallite size L given by the Scherrer equation is $V^{1/3}$, which is a volumetric average.[17] The dimension of the octahedra that we estimated from the TEM micrographs was the distance between opposite vertices. This distance, whose average was found to be 54 nm, is the greatest length inside the volume determined by an octahedron. Then, the average edge "a" of the octahedra (see Figure 2) in our sample measured 38 nm, and the average volume ($V = (1/3)2^{1/2}a^3$) was approximately 25 900 nm^3. The volumetric average is then 29 nm, which agrees very well with the apparent crystallite dimension calculated using the Scherrer equation, and is further evidence that our magnetite sample consisted mostly of monocrystalline particles.

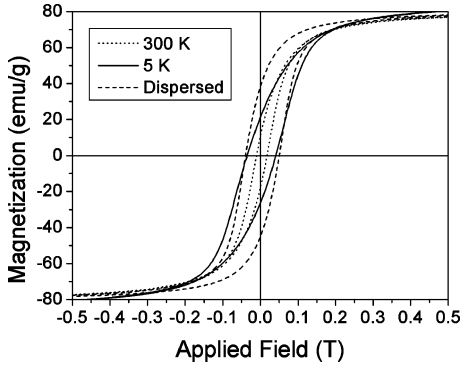

Figure 7. Magnetization as a function of applied field for a powder sample of the magnetite octahedral particles as prepared at room temperature and at 5 K, and for the same particles dispersed in a silica matrix at room temperature.

3.3. Magnetic Properties. In Figure 7 we show the hysteresis loop corresponding to iron oxide powder at 300 K. Assuming a magnetite bulk density of 5.17 g/mL, a saturation magnetization of 422 kA/m (81.6 emu/g) was measured. This represents 89% of the value of 475 kA/m for bulk magnetite.[28] Surface effects, such as spin canting, partial oxidation, and deviations from stoichiometry or adsorbed molecules are usually held responsible for values of M_s smaller than that for the bulk material. Surface effects become more important as the average size of the particles decreases, and therefore explain why lower values of M_s are observed the smaller the particle size becomes. For instance, our group measured the 475 kA/m for micrometer sized magnetite particles,[29] whereas Daou et al.[3] observed 427 kA/m for 39 nm magnetite particles. Goya et al.[30] observed this tendency in a collection of four samples with particle sizes that ranged from 5 to 150 nm.

Hysteresis loops were also measured for iron oxide powders for a range of different temperatures down to 5 K. By way of example, in Figure 7, the curves corresponding to 5 and 300 K are shown. From these curves, coercivity and M_s/M_r are measured and plotted in Figure 8, parts a and b, respectively. As observed in Figure 8a, particle coercivity increases from 140 to 380 Oe at low temperature and goes up to 450 Oe when dispersed in the silica network. The variation of the coercivity with both temperature and packing fraction depends on the kind of anisotropy present. Thus, variation of the coercivity with temperature points out that crystal anisotropy is contributing to the coercivity since shape anisotropy constant is independent of temperature. However, coercivity also depends on the packing fraction, increasing as the packing fraction decreases because of the reduction in particle interactions. This means that shape anisotropy is also contributing to the coercivity. When crystal anisotropy prevails, the coercivity is expected to be independent of the packing fraction since this anisotropy is due to forces (spin−orbit coupling) which are internal to the particle and not, as is the case with shape anisotropy, to magnetostatic fields external to the particle.[31]

Finally, it should be mentioned that the coercivity values of the dispersed particles were larger than those expected for uniaxial single-domain non-interacting spherical particles whose magnetization reverses by coherent rotation following the Stoner−Wohlfarth model. The predicted value would be around 300 Oe ($H_c = \phi_p K_1/M_s$, where ϕ_p is equal to 0.64 for a random assembly of particles, K_1 is the crystal anisotropy for magnetite, and M_s is the saturation magnetization).[32] Only the fact that the particles are anisometric could account for the coercivity value of 450 Oe, which has been previously measured for elongated

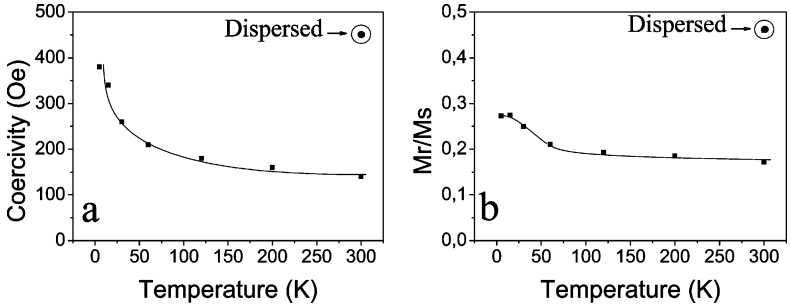

Figure 8. Variation of the coercivity (a) and the squareness (b) of the loop with the temperature for magnetite octahedral particles as prepared. The lines are a guide to the eye. Results are also shown for particles dispersed in a silica matrix at room temperature.

particles for which the rotation of the magnetization took place by incoherent mechanisms.[19]

The hysteresis loop squareness, measured by the M_r/M_s ratio, increases from 0.2 to 0.3 at low temperature as a consequence of the thermal energy reduction. It should be noted that the theoretical value for uniaxial single-domain particles, distributed at random and non-interacting would be 0.5[31] and this value is only reached when the particles are dispersed in the silica matrix due to a reduction in cooperative effects. The squareness of the magnetization loop of the dispersed particles suggests that when the particle interactions are neglected, coherent rotation is the most probable mechanism of magnetization reversal in these particles.

The mechanism by which the magnetization of a particle varies, changes from domain wall rotation to spin rotation as the particle size is reduced. For large sizes, the particle behaves as multidomain units and the magnetization changes by domain wall motion even if the particle is a monocrystal. Small domains of reversed magnetization will be present near imperfections at the surface or small scale inhomogeneities in the chemical composition of the particle. However, below a critical diameter which is not well defined, the particles become single domains and change their magnetization by either coherent or incoherent spin rotation, depending on whether or not spins of all atoms in the particle remain parallel to one another during rotation. The critical size for magnetite seems to be around 30−50 nm, or slightly above that range if the particles are elongated.[33,30] Furthermore, for magnetite particles with diameters below 10 nm, thermal energy will tend to disalign the magnetic moments of the particles leading to a superparamagnetic behavior, with zero coercivity and no remanence magnetization.[34]

In this work, the single domain character of the octahedral particles of 54 nm, and hence their monocrystalline structure, has been evidenced by the high coercivity and high squareness of the magnetization loop when particles were isolated in the silica matrix.

4. Conclusions

The oxidative aging of $Fe(OH)_2$ in the presence of KNO_3 is a known method for the fabrication of several iron oxides and hydroxides. We reported a set of conditions that yielded uniform single-domain monocrystalline octahedral magnetite particles. An average distance of 54 ± 14 nm between opposite vertices of the octahedra was estimated from TEM micrographs. Characterization of these particles confirmed that they were single crystals with a composition that was close to the theoretical stoichiometry of magnetite, a ferrimagnetic behavior at room temperature and a saturation magnetization of 422 kA/m.

Enhanced crystal anisotropy coming from the well-defined crystal structure and shape anisotropy due to the slight anisotropy of the particles seems to be responsible for the ferrimagnetic behavior of the particles, leading to coercivity values of 450 Oe at room temperature when particle interactions are neglected. Particles behave as single domains and coherent rotation seems to be the most probable mechanism of magnetization reversal in these particles, in spite of having a diameter in the vicinity of that predicted to be the boundary between the single-domain and the multidomain behavior.

Acknowledgment. The authors would like to thank F. Galisteo-González for providing the Bool2k software used for the generation of particle-size distributions from TEM micrographs, and Alejandro Rodriguez Navarro, from the Department of Mineralogy and Petrology of the University of Granada, for helpful discussions. This work was supported by MEC MAT-2006-13646-C03-03 and MAT-2005-03179 projects (Spain), by the European Regional Development Fund (ERDF), and by Junta de Andalucía FQM 392 and P07-FQM-2496 projects (Spain).

References and Notes

(1) Shinkai, M. *J. Biosci. Bioeng.* **2002**, *94*, 606.
(2) Charles, S. W. In *Ferrofluids*; Odenbach, S., Ed.; Springer-Verlag: Berlin, 2002.
(3) Daou, T. J.; Pourroy, G.; Begin-Colin, S.; Greneche, J. M.; Ulhaq-Bouillet, C.; Legare, P.; Bernhardt, P.; Leuvrey, C.; Rogez, G. *Chem. Mater.* **2006**, *18*, 4399.
(4) Ma, M.; Wu, Y.; Zhou, J.; Sun, Y.; Zhang, Y.; Gu, N. *J. Magn. Magn. Mater.* **2004**, *268*, 33.
(5) Domingo, C.; Rodriguez-Clemente, R.; Blesa, M. A. *Mater. Res. Bull.* **1991**, *26*, 47.
(6) Sugimoto, T.; Matijević, E. *J. Colloid Interface Sci.* **1980**, *74*, 227.
(7) Regazzoni, A. E.; Matijević, E. *Corrosion* **1982**, *38*, 212.
(8) Regazzoni, A. E.; Matijević, E. *Colloid Surf. A* **1983**, *6*, 189.
(9) Tamura, H.; Matijević, E. *J. Colloid Interface Sci.* **1982**, *90*, 100.
(10) Domingo, C.; Rodriguez-Clemente, R.; Blesa, M. A. *Colloid Surf. A* **1993**, *79*, 177.
(11) Domingo, C.; Rodriguez-Clemente, R.; Blesa, M. *J. Colloid Interface Sci.* **1994**, *165*, 244.
(12) Spiers, K. M.; Forsythe, J. S.; Suzuki, K.; Cashion, J. D. *J. Magn. Magn. Mater.* **2007**, *311*, 97.
(13) Zhang, L. Y.; Gu, H. C.; Wang, X. M. *J. Magn. Magn. Mater.* **2007**, *311*, 228.
(14) Yang, J. B.; Zhou, X. D.; Yelon, W. B.; James, W. J.; Cai, Q.; Gopalakrishnan, K. V.; Malik, S. K.; Sun, X. C.; Nikles, D. E. *J. Appl. Phys.* **2004**, *95*, 7540.
(15) Devouard, B.; Posfai, M.; Hua, X.; Bazylinski, D. A.; Frankel, R. B.; Buseck, P. R. *Am. Mineral.* **1998**, *83*, 1387.
(16) Altermatt, U. D.; Brown, I. D. *Acta Crystallogr. A* **1987**, *43*, 125.
(17) Guinier, A. In *X-Ray Diffraction in Crystals, Imperfect Crystals, and Amorphous Bodies*; Dover Publications, Inc: Mineola, New York, 1994; Chapter 5.
(18) *www.xpowder.com*
(19) Morales, M. P.; Muñoz-Aguado, M. J.; García-Palacios, J. L.; Lázaro, F. J.; Serna, C. J. *J. Magn. Magn. Mater.* **1998**, *183* (1−2), 232.
(20) Parks, G. A. *Chem. Rev.* **1965**, *65*, 177.
(21) Dutta, P.; Manivannan, A.; Seehra, M. S.; Shah, N.; Huffman, G. P. *Phys. Rev. B* **2004**, *70*, 174428.

(22) Jorgensen, J. E.; Mosegaard, L.; Thomsen, L. E.; Jensen, T. R.; Hanson, J. C. *J. Solid State Chem.* **2007**, *180*, 180.

(23) Belin, T.; Guigue-Millot, N.; Caillot, T.; Aymes, D.; Niepce, J. C. *J. Solid State Chem.* **2002**, *163*, 459.

(24) Morales, M. P.; Pecharroman, C.; Gonzalez Carreño, T.; Serna, C. J. *J. Solid State Chem.* **1994**, *108*, 158.

(25) Xiong, Y.; Ye, J.; Gu, X. Y.; Chen, Q. W. *J. Phys. Chem. C* **2007**, *111*, 6998.

(26) Shebanova, O. N.; Lazor, P. *J. Solid State Chem.* **2003**, *174*, 424.

(27) Chamritski, I.; Burns, G. *J. Phys. Chem. B* **2005**, *109*, 4965.

(28) Cabuil, V. In *Encyclopedia of Surface and Colloid Science*; Hubbard, A. T., Ed.; Marcel Dekker Ltd: New York, 2002.

(29) Vereda, F.; de Vicente, J.; Hidalgo-Álvarez, R. *Langmuir* **2007**, *23*, 3581.

(30) Goya, G. F.; Berquo, T. S.; Fonseca, F. C.; Morales, M. P. *J. Appl. Phys.* **2003**, *94*, 3520.

(31) Cullity, B. D. In *Introduction to Magnetic Materials*; Addison-Wesley: Reading, MA, 1972.

(32) Stone, E. C.; Wohlfarth, E. P. *Philos. Trans. R. Soc. London, Ser. A* **1948**, *A-240*, 599.

(33) Prozorov, T.; Mallapragada, S. K.; Narasimhan, B.; Wang, L.; Palo, P.; Nilsen-Hamilton, M.; Williams, T. J.; Bazylinski, D. A.; Prozorov, R.; Canfield, P. C. *Adv. Funct. Mater.* **2007**, *17* (6), 951.

(34) Morales, M. P.; Veintemillas-Verdaguer, S.; Montero, M. I.; Serna, C. J.; Roig, A.; Casas, L.; Martínez, B.; Sandiumenge, F. *Chem. Mater.* **1999**, *11* (11), 3058.